ELSEVIER

Journal of Analytical and Applied Pyrolysis
62 (2002) 45–62

JOURNAL of ANALYTICAL and APPLIED PYROLYSIS

www.elsevier.com/locate/jaap

Thermogravimetry and X-ray diffraction study of the thermal decomposition processes in Li_2CO_3–$MnCO_3$ mixtures

V. Berbenni *, A. Marini

C.S.G.I., Dipartimento di Chimica Fisica dell'Università di Pavia, Viale Taramelli 16 27100, Pavia, Italy

Received 7 August 2000; accepted 16 November 2000

Abstract

The thermal decomposition processes taking place in solid state mixtures Li_2CO_3–$MnCO_3$ ($x_{Li} = 0.10$–0.50, x_{Li} = lithium cathionic fraction) have been studied (both in air and nitrogen flow) by thermogravimetric analysis (TGA), in order to get a better understanding of the different possible by-products, and by X-ray powder diffractometry (XRD) to assess the equilibrium compounds. As concerns the measurements performed in air, $LiMn_2O_4$ and excess Mn_2O_3 are the equilibrium products obtained for x_{Li} up to 0.33. By $0.33 < x_{Li} < 0.50$ a mixture of $LiMn_2O_4$ and Li_2MnO_3 is obtained. In this case the TGA data show that an excess lithiated spinel phase ($Li_{1+x}Mn_2O_4$) is obtained as an intermediate phase. The measurements performed in nitrogen (x_{Li} up to 0.33) show, when examined by TGA, the formation reaction of $LiMn_2O_4$ and Mn_3O_4 which is completed within about 720°C. At higher temperatures a rather complex reaction takes place between $LiMn_2O_4$ and the excess Li_2O present at 720°C, leading to the formation of the compounds $Li_2Mn_2O_4$ and $LiMnO_2$ again with excess of Mn_3O_4. At higher mixture lithium content ($0.33 < x_{Li} < 0.50$) $LiMn_2O_4$, Li_2MnO_3 and Mn_3O_4 form up to about 720°C. At higher temperatures $LiMnO_2$ is by far the majority phase present which is formed by solid state reactions occurring between $LiMn_2O_4$ and Li_2MnO_3 and between Li_2MnO_3 and Mn_3O_4.

Keywords: Lithium manganese oxides; Thermogravimetric analysis (TGA); Thermal decomposition; Li_2CO_3; $MnCO_3$

* Corresponding author. Tel.: +39-382-507211; fax: +39-382-507575.
E-mail address: berbenni@fisav.unipv.it (V. Berbenni).

0165-2370/02/$ - see front matter
PII: S0165-2370(00)00211-4

1. Introduction

Manganese oxides with tunnel or layered structures have attracted considerable attention owing to their application as selective adsorbents [1], cathode materials for advanced lithium batteries [2–6] and catalysts [7,8]. A phase diagram of the Li–Mn–O system has been reported in [9].

In particular the compounds $LiMnO_2$ (orthorombic structure) [10] and $LiMn_2O_4$ (cubic spinel structure) [11] have been regarded to be promising candidates as hosts for the deintercalation/intercalation of lithium from/into cathodes of Li-batteries. This is due to their lower cost and toxicity as compared to the oxides of cobalt, nickel or vanadium. Extensive research on how these compounds behave, under various operating conditions and configurations in Li cells, has been performed and still is underway [12–15].

The electrochemical studies have been accompanied by a widespread physicochemical characterization. Actually the requirements that must be satisfied by a solid, if it is to be successful as a positive electrode in rechargeable lithium batteries, are very demanding [16–19]. Furthermore new preparation routes have been proposed particularly for $LiMn_2O_4$ [20–22] alternative to solid state synthesis.

Solid state formation of $LiMn_2O_4$ and $LiMnO_2$ has been accomplished starting from different reacting systems (mainly Li_2CO_3 and MnO_2) and the obtained products have been thoroughly characterized also from the point of view of their thermal stability [23–25].

The aim of the present work is an examination of the thermal decomposition processes taking place in the solid state mixtures Li_2CO_3–$MnCO_3$ to assess which are the compounds that form depending both on starting composition and working atmosphere (air and nitrogen atmospheres). Such a task has been pursued by using thermogravimetric analysis (TGA) to examine the intermediate stages of the reaction over the heating ramp and X-ray powder diffractometry (XRD) to assess the equilibrium compounds formed.

2. Experimental

2.1. Samples preparation

Mixtures of Li_2CO_3 (99.99%, Aldrich, Italy) and $MnCO_3$ (99.9%, Aldrich, Italy) in the composition range $x_{Li} = 0.10$–0.50 in steps of 0.05 units (x_{Li} = lithium cathionic fraction) have been prepared by weighing the appropriate amounts of the two components (up to about 2 g of each mixture). Afterwards the physical mixtures have been prepared by suspending the powders under magnetic stirring in acetone for 3 h. Then the solvent has been let to evaporate in oven at 40°C.

2.2. Experimental apparatus

The solid state processes occurring in the sample mixtures have been followed by thermogravimetric analysis (TGA 2950 by TA Intruments Ltd. USA connected to TA5000 Computer also by TA Instruments equipped with Thermal Solutions™ software). The TG measurements have been performed, on samples of about 20 mg, at a heating rate of 2°C min^{-1} in the temperature range 25–850°C both in air and nitrogen flow (100 ml min^{-1}). Samples of the same mixtures (about 500 mg of each sample) have been allowed to react in a furnace (Stanton Redcroft, UK T_{max} 1700°C) by heating them at 2°C min^{-1} up to 850°C (both in air and nitrogen flow). An isothermal stage of 16 h at 850°C has been appended to the heating ramp. All the samples annealed in the furnace have been examined by X-ray diffraction. Use has been made of a Bruker Powder Diffractometer D5005 (2ϑ range = 15–70°, CuKα radiation, step scan mode, step width 0.02°, counting time 3 s, 40 kV, 40 mA).

3. Results and discussion

3.1. Thermal decomposition performed in flowing air

3.1.1. Pure $MnCO_3$

The possible decomposition routes of $MnCO_3$ are the following (the relevant mass losses in mass% are also reported):

1. $MnCO_3\ (s) \rightarrow MnO\ (s) + CO_2\ (g) \quad \Delta M_1 = -38.29$
2. $MnCO_3\ (s) + (1/6)O_2\ (g) \rightarrow (1/3)Mn_3O_4\ (s) + CO_2\ (g) \quad \Delta M_2 = -33.65$
3. $MnCO_3\ (s) + (1/4)O_2\ (g) \rightarrow (1/2)\ Mn_2O_3\ (s) + CO_2\ (g) \quad \Delta M_3 = -31.33$
4. $MnCO_3\ (s) + (1/2)O_2\ (g) \rightarrow MnO_2\ (s) + CO_2\ (g) \quad \Delta M_4 = -24.37$

Four independent scans (2°C min^{-1}, 25–850°C) have been performed on pure manganese carbonate samples whose results are reported in Table 1.

It can be seen that the reaction is over at a temperature (T_1) which lies well below the maximum operating temperature (850°C). Indeed the mean mass loss value ($-32.10 \pm 0.03\%$ at T_1 and $-32.12 \pm 0.05\%$ at 850°C) falls between ΔM_2 and ΔM_3. It can be easily calculated that a -32.10% value corresponds to a residue

Table 1
Pure $MnCO_3$ decomposition in air[a]

ΔM_{T_1} (%)	T_1 (°C)	ΔM_{850} (%)
−32.14	575.47	−32.19
−32.10	567.36	−32.13
−32.09	568.98	−32.09
−32.06	578.72	−32.07

[a] TGA data.

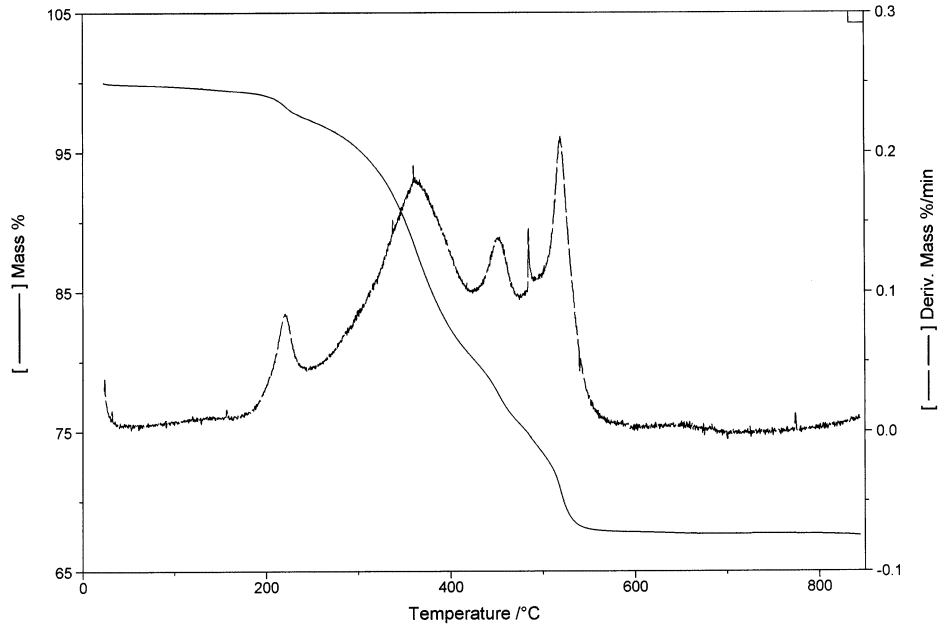

Fig. 1. TG thermogram of the $x_{Li} = 0.2018$ mixture heated in flowing air. Both mass signal (in %) and its derivative with respect to time (in % min^{-1}) are reported vs. temperature.

which, under the experimental conditions utilized in the work, would be constituted (in mass%) by 32.24 of Mn_3O_4 and 67.60 of Mn_2O_3.

3.1.2. Li_2CO_3–$MnCO_3$ mixtures ($x_{Li} = 0.10$–0.33)

A TGA measurement (mixture composition $x_{Li} = 0.2018$), whose trend is typical of all measurements performed in this specific composition range, is reported in Fig. 1. The experimental mass losses recorded both at 600°C ($\Delta M_{600°C}$) and at 850°C ($\Delta M_{850°C}$) are reported in Table 2. ΔM_{calc} is the mass loss calculated according to the following reaction scheme:

Table 2
TGA results (air flow) on mixtures in the composition range $x_{Li} = 0.10$–0.33[a]

x_{Li}	$\Delta M_{600°C}$ (%)	$\Delta M_{850°C}$ (%)	ΔM_{calc} (%)
0.0998	-32.06 ± 0.30	-32.19 ± 0.55	-32.13
0.1502	-32.31 ± 0.15	-32.59 ± 0.42	-32.15
0.2018	-32.23 ± 0.35	-32.83 ± 0.51	-32.18
0.2507	-32.22 ± 0.26	-32.92 ± 0.23	-32.20
0.2997	-32.17 ± 0.19	-32.92 ± 0.50	-32.22
0.3338	-32.62 ± 0.13	-33.45 ± 0.30	-32.30

[a] The experimental mass losses at 600°C ($\Delta M_{600°C}$) and at 850°C ($\Delta M_{850°C}$) are the mean of three independent runs. ΔM_{calc} represents the mass loss calculated under the hypothesis of reaction Eq. (I) plus excess $MnCO_3$ decomposition.

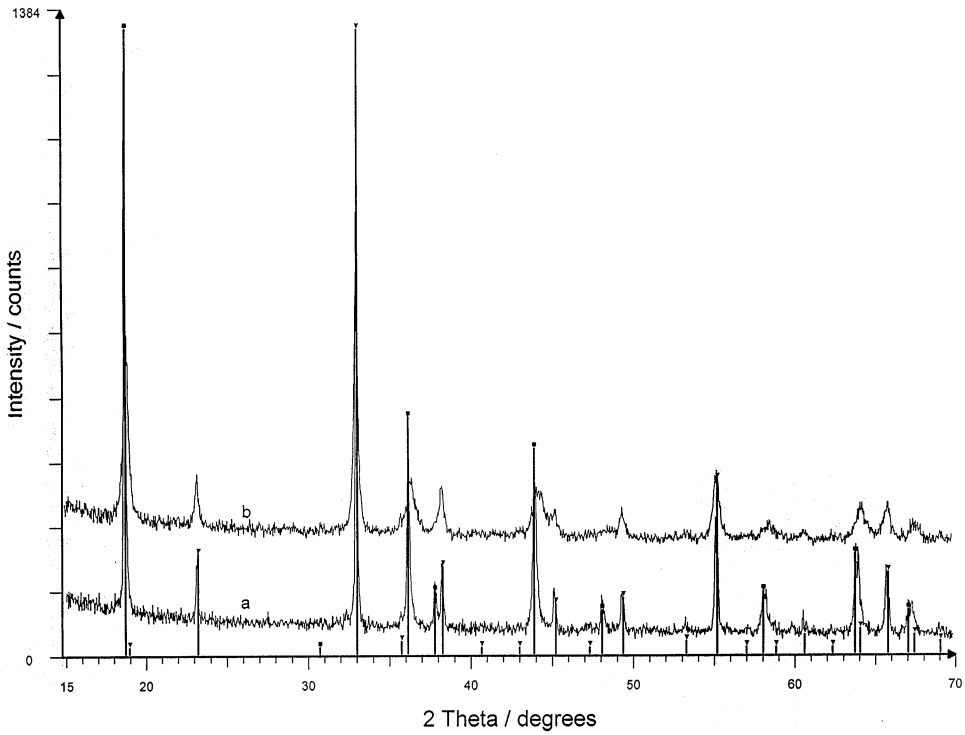

Fig. 2. XRD powder patterns of the $x_{Li} = 0.2018$ mixture heated in flowing air (furnace). Trace *a*: maximum temperature 850°C. Trace *b*: maximum temperature 600°C. Squares represent $LiMn_2O_4$ (JCPDS card n.35-0782); Triangles represent Mn_2O_3 patterns (JCPDS card n. 41-1442).

$$\left(\frac{x_{Li}}{2}\right)Li_2CO_3 + 2x_{Li}MnCO_3 + \left(\frac{3x_{Li}}{4}\right)O_2(g) \rightarrow x_{Li}LiMn_2O_4 + \left(\frac{5x_{Li}}{2}\right)CO_2(g) \quad \text{(I)}$$

(Note that the stoichiometric coefficients are expressed in terms of x_{Li} so that the mass variations pertaining to the reaction can be directly calculated for the different mixture compositions) and by taking also into account that the excess $MnCO_3$ (namely $1 - 3x_{Li}$ moles) decomposes as pure $MnCO_3$ does (i.e. to a mixture of Mn_3O_4 and Mn_2O_3). It can be seen that the experimental-calculated differences are almost negligible at 600°C while they tend to slightly increase at 850°C. While it is unlikely that the anionic close packed arrangement of the lithium manganese spinel ($LiMn_2O_4$) would allow oxygen substoichiometry, it is reasonable to consider that at $T > 600$°C the oxygen activity decreases with the result that the excess Mn_2O_3 slightly reduces to Mn_3O_4.

Fig. 2 reports the XRD patterns of the mixture $x_{Li} = 0.2018$ heated in air at 2°C min^{-1} up to 600°C (b) and 850°C (a). The reflections of $LiMn_2O_4$ and Mn_2O_3 are the only ones which are present at both temperatures. The only difference is the improved crystallization at 850°C as it is revealed by the sharper peaks present in

the a trace. Therefore, the XRD patterns of the mixtures up to $x_{Li} = 0.33$ heated in air confirm that the compound $LiMn_2O_4$ forms already within 600°C. On the other hand it can be concluded that the route of the excess $MnCO_3$ decomposition is different with respect to that it takes when it is carried out in TGA apparatus. As a matter of fact no Mn_3O_4 is present in the mixtures which have been heated for a prolonged time in the furnace. This fact could be due to a somewhat lower oxygen activity in the TGA oven.

3.1.3. Li_2CO_3–$MnCO_3$ mixtures ($x_{Li} = 0.35$–0.50)

Fig. 3 reports a TGA run (mixture $x_{Li} = 0.4001$) whose trend is typical of all measurements performed in this specific composition range. The main difference with respect to the TGA runs performed on the sample mixtures of the lower composition range (see Section 3.1.2) lies with the fact that the mass loss proceeds up to temperatures above 700°C (indicated as T_2 in the following). Table 3 reports the mass losses at T_2, the relevant T_2 values and the mass losses at 850°C.

By taking into account the composition range and the fact that no Mn oxide(s) excess is present in the XRD patterns of the reacted mixtures, two models of the reaction taking place can be proposed:

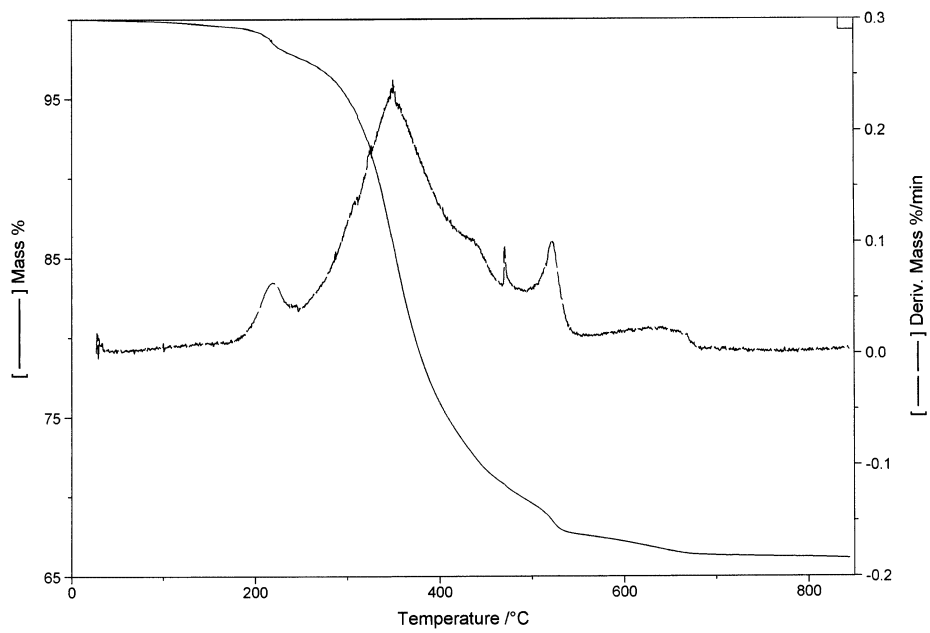

Fig. 3. TG thermogram of the $x_{Li} = 0.4001$ mixture heated in flowing air. Both mass signal (in %) and its derivative with respect to time (in % min^{-1}) are reported vs. temperature.

Table 3
TGA results (air flow) on the mixtures in the composition range $x_{Li} = 0.35$–0.50[a]

x_{Li}	ΔM_{T_2} (%)	T_2 (°C)	ΔM_{850} (%)	ΔM_{carb} (%)	w_{O_2}	$1+x$	ΔM_{II} (%)	ΔM_{III} (%)
0.3501	−33.53	696.92	−33.62	−41.43	0.21637	1.2552	−32.76	−32.45
0.4001	−33.70	708.57	−33.87	−42.04	0.21625	1.1574	−34.40	−33.13
0.4503	−34.70	737.91	−34.81	−42.72	0.20007	1.2625	−36.21	−33.87
0.5008	−35.12	716.79	−35.19	−43.47	0.19802	1.1724	−38.23	−34.70

[a] ΔM_{T_2} are the experimental mass losses at T_2. ΔM_{carb} are the mass losses calculated on the basis of the mere carbonates decomposition. w_{O_2} is the O_2 intake (in moles) of the mixtures. ΔM_{II} and ΔM_{III} are the mass losses calculated according to reaction models Eq. (II) and Eq. (III), respectively. $1+x$ is the stoichiometric index of the lithiated spinel formed according to reaction model Eq. (IV).

- $$\left(\frac{x_{Li}}{2}\right)Li_2CO_3 + (1-x_{Li})MnCO_3 + \left(\frac{2-3x_{Li}}{4}\right)O_2(g) \rightarrow (1-2x_{Li})LiMn_2O_4 + (3x_{Li}-1)LiMnO_2 + \left(\frac{2-x_{Li}}{2}\right)CO_2(g) \quad \text{(II)}$$

  The mass losses calculated according to the above reaction are reported in Table 3 (ΔM_{II}).

- $$\left(\frac{x_{Li}}{2}\right)Li_2CO_3 + (1-x_{Li})MnCO_3 + \left(\frac{4-3x_{Li}}{12}\right)O_2(g) \rightarrow \left(\frac{2-3x_{Li}}{3}\right)LiMn_2O_4 + \left(\frac{3x_{Li}-1}{3}\right)Li_2MnO_3 + \left(\frac{2-x_{Li}}{2}\right)CO_2(g) \quad \text{(III)}$$

  The mass losses calculated according to the above reaction are reported in Table 3 (ΔM_{III}).

It can be seen that reaction II does not yield mass loss data that satisfactorily agree with the experimental ones while such an agreement is somewhat better in the case of reaction III even if the experimental mass losses are still higher (in all but the $x_{Li} = 0.3501$ mixture) than the calculated ones.

Fig. 4 reports the XRD patterns of the mixtures heated at 2°C min^{-1} up to 850°C and annealed for 16 h. While only $LiMn_2O_4$ reflections (squares) are present in the $x_{Li} = 0.3501$ mixture, characteristic Li_2MnO_3 reflections (circles) at $2\theta \approx 37, 44.5$ and 65.5° appear starting from the $x_{Li} = 0.4001$ mixture.

No $LiMnO_2$ reflections appear, so that reaction II can be definitely ruled out also by XRD experiments.

What it is likely to occur in this composition range, is the formation of an excess lithiated spinel $Li_{1+x}Mn_2O_4$ (this fact would account for the mass loss greater than expected on the basis of reaction III) and Li_2MnO_3 according to the reaction model IV:

$$\left(\frac{x_{\mathrm{Li}}}{2}\right)\mathrm{Li_2CO_3} + (1-x_{\mathrm{Li}})\mathrm{MnCO_3} + w\mathrm{O_2(g)} \rightarrow \left(\frac{4-4w_{\mathrm{O_2}}-5x_{\mathrm{Li}}}{4}\right)\mathrm{Li_{1+x}Mn_2O_4} + \left(\frac{3x_{\mathrm{Li}}-2+4w_{\mathrm{O_2}}}{2}\right)\mathrm{Li_2MnO_3} + \left(\frac{2-x_{\mathrm{Li}}}{2}\right)\mathrm{CO_2(g)} \quad \text{(IV)}$$

where $w_{\mathrm{O_2}} = ((\Delta M_{T_2} - \Delta M_{\mathrm{carb}})/M_{\mathrm{O_2}}100) \times M_{\mathrm{tot,mix}}$ represents the intake of oxygen (in moles) of the mixtures and $M_{\mathrm{tot,mix}}$ is the total mass of the mixture.

Hence from the mass losses at T_2 (ΔM_{T_2}) and from the losses expected on the basis of the carbonates decomposition (ΔM_{carb}), the values of $1+x$ can be calculated (see Table 3). It is important here to note that the formation of the excess lithiated spinel ($\mathrm{Li_{1+x}Mn_2O_4}$) has been considered to fully explain the thermogravimetric results. It seems that the equilibrium situation (see the XRD results reported in Fig. 4) does not need to invoke its presence. Enough furnace annealing time in air has been evidently allowed to get fully oxidized, stoichiometric $\mathrm{LiMn_2O_4}$ as the equilibrium compound along with monoclinic $\mathrm{Li_2MnO_3}$.

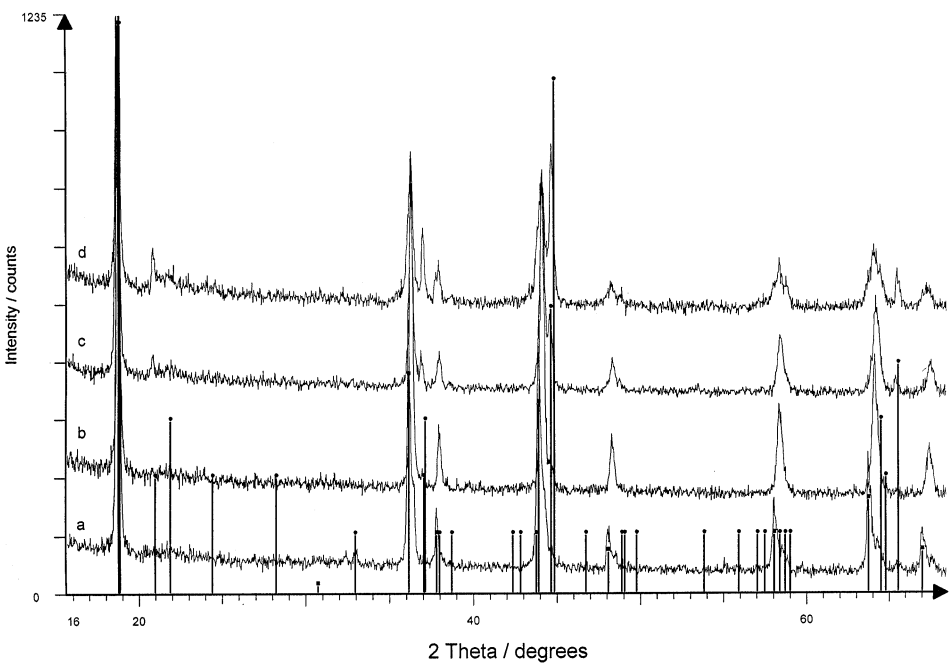

Fig. 4. XRD powder patterns of the mixtures with $x_{\mathrm{Li}} > 0.33$ heated in air up to 850°C. (a) $x_{\mathrm{Li}} = 0.3501$; (b) $x_{\mathrm{Li}} = 0.4001$; (c) $x_{\mathrm{Li}} = 0.4503$; (d) $x_{\mathrm{Li}} = 0.5008$. Squares represent $\mathrm{LiMn_2O_4}$ patterns (JCPDS card n. 35-0782); Circles represent $\mathrm{Li_2MnO_3}$ patterns (JCPDS card n. 27-1252).

Table 4
$MnCO_3$ decomposition in nitrogen[a]

Mass (mg)	ΔM_{600} (%)	ΔM_{T_2} (%)	T_2 (°C)	ΔM_{850} (%)
27.072	−34.82	−34.48	716.68	−34.53
32.420	−34.38	−34.43	700.45	−34.44
19.897	−33.65	−34.47	723.17	−34.47
17.421	−33.51	−34.34	731.28	−34.32

[a] TGA data.

3.2. Thermal decomposition performed in flowing nitrogen

3.2.1. Pure $MnCO_3$

Four measurements (2°C min^{-1} 25–850°C) have been performed on pure $MnCO_3$ samples whose results are reported in Table 4. From the data it can be seen that Mn_3O_4 ($\Delta M = -33.65\%$) forms at 600°C, within the experimental error, provided sample mass is lower enough (less than about 20 mg) so as to allow oxygen interaction within the decomposing solid. At $T > 600$°C a partial manganese reduction takes place which ends within T_2 (the mean % mass loss is −0.82%). The total mean % mass loss value at T_2 is $-34.43 \pm 0.06\%$ which corresponds to a residue constituted by 15.9% (by mass%) of MnO and the balance Mn_3O_4. Fig. 5 (trace *a*) shows the XRD patterns of a $MnCO_3$ sample treated in a furnace under the same experimental conditions adopted in TGA analysis. For sake of comparison the XRD patterns of commercial Mn_3O_4 are also reported (trace *b*) It can be seen that, besides the reflections pertaining to Mn_3O_4, two peaks are also present which can be surely attributed to MnO (see the peaks at $2\vartheta = 35°$ and 41° in trace *a*). Therefore, it can be concluded that the oxidation extent under nitrogen is lower than that leading to Mn_3O_4.

3.2.2. Li_2CO_3–$MnCO_3$ mixtures ($x_{Li} = 0.10$–0.33)

A TGA scan (mixture $x_{Li} = 0.2018$) whose trend is typical of all measurements performed in this specific composition range is reported in Fig. 6.

The experimental data reported in Table 5 are the mean of four independent runs performed on each mixture composition. The ΔM_A and ΔM_B values are the mass loss values that have to be expected in the case of the reaction schemes A and B:

$$\left(\frac{x_{Li}}{2}\right)Li_2CO_3 + (1 - x_{Li})MnCO_3 + \left(\frac{2 + 3x_{Li}}{12}\right)O_2(g)$$
$$\rightarrow\ x_{Li}\,LiMn_2O_4 + \left(\frac{1 - 3x_{Li}}{3}\right)Mn_3O_4 + \left(\frac{2 - x_{Li}}{2}\right)CO_2(g) \qquad \text{(scheme A)}$$

$$\left(\frac{x_{Li}}{2}\right)Li_2CO_3 + (1 - x_{Li})MnCO_3 + \left(\frac{2 - x_{Li}}{12}\right)O_2(g)$$
$$\rightarrow\ x_{Li}\,LiMnO_2 + \left(\frac{1 - 2x_{Li}}{3}\right)Mn_3O_4 + \left(\frac{2 - x_{Li}}{2}\right)CO_2(g) \qquad \text{(scheme B)}$$

As concerns the data reported in Table 5 the following considerations apply:

1. the mass loss data at T_2 (which represents a temperature which is in any case above that of lithium carbonate spontaneous decomposition i.e. ≈ 640°C) lay between ΔM_A and ΔM_B;
2. a further, sensible mass loss process takes place at $T > T_2$ which ends just below 850°C;
3. the mass loss data at 850°C are in all cases slightly higher than the correspondent ΔM_B values.

Point i) could be explained by the formation of a mixture of MnO and Mn_3O_4 plus $LiMn_2O_4$ (model A). However, it can be easily verified that the difference between ΔM_{T_2} and ΔM_A increases with increasing x_{Li} i.e. with decreasing Mn content of the mixtures. Another explanation could be found by admitting the formation of a mixture of $LiMnO_2$ and $LiMn_2O_4$ plus excess Mn_3O_4. However, XRD measurements performed on the residues of TGA runs carried out up to 600°C allowed to verify that only MnO, Mn_3O_4 and $LiMn_2O_4$ were present. No $LiMnO_2$ was definitely found.

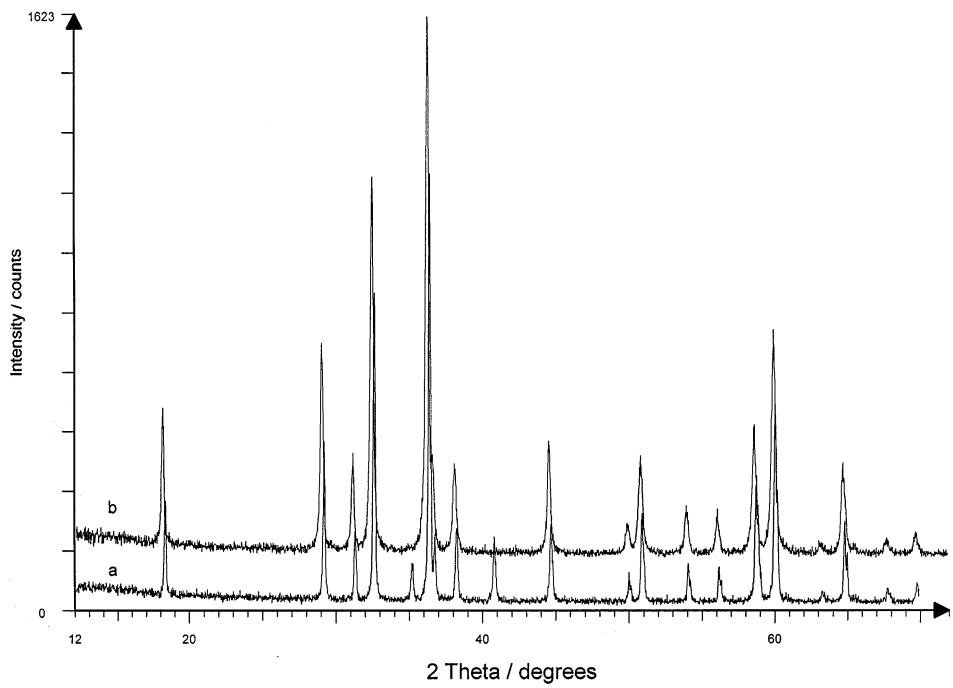

Fig. 5. XRD powder patterns of: (a) $MnCO_3$ heated in flowing nitrogen up to 850°C; (b) commercial Mn_3O_4 sample.

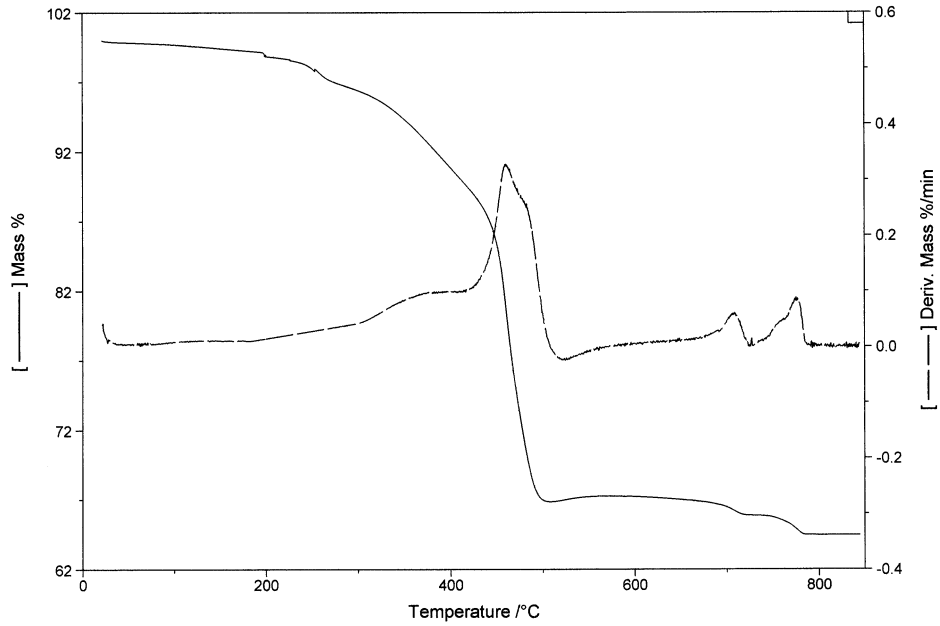

Fig. 6. TG thermogram of the $x_{Li} = 0.2018$ mixture heated in flowing nitrogen. Both mass signal (in %) and its derivative with respect to time (in % min^{-1}) are reported vs. temperature.

On the other hand point ii) implies that, under nitrogen flow, one or more of the compounds that have been formed within T_2, are not stable at higher temperatures.

The fact that the total mass loss at 850°C is fairly close to the ΔM_B values at each composition (point iii), suggests that the process taking place between T_2 and 850°C could be the decomposition of $LiMn_2O_4$ to yield $LiMnO_2$ according to the reaction scheme:

Table 5
TGA results (nitrogen flow) on the mixtures in the composition range $x_{Li} = 0.10$–0.33[a]

x_{Li}	ΔM_{T_2} (%)	T_2 (°C)	ΔM_{850} (%)	ΔM_A(%)	ΔM_B (%)	ΔM_{HT}
0.0998	-34.19 ± 0.13	732	-35.02 ± 0.07	-33.30	-34.29	-0.76 ± 0.01
0.1502	-34.01 ± 0.23	723	-35.30 ± 0.03	-33.10	-34.65	-1.29 ± 0.21
0.2018	-33.94 ± 0.17	724	-35.64 ± 0.07	-32.88	-35.05	-1.70 ± 0.23
0.2507	-33.74 ± 0.21	720	-35.95 ± 0.11	-32.66	-35.46	-2.22 ± 0.17
0.2997	-33.86 ± 0.18	710	-36.47 ± 0.21	-32.42	-35.91	-2.62 ± 0.13
0.3338	-34.05 ± 0.02	715	-36.81 ± 0.13	-32.24	-36.24	-2.77 ± 0.12

[a] The experimental mass losses at T_2 (ΔM_{T_2}), at 850°C ($\Delta M_{850°C}$) and between T_2 and 850°C (ΔH_{HT}) are the mean of four independent runs. ΔM_A and ΔM_B are the mass losses calculated under reaction schemes Eq. (A) and Eq. (B).

Table 6
The n values represent the number of $LiMn_2O_4$ moles formed up to T_2 and calculated from the experimental ΔM_{HT} values[a]

X_{Li}	N	$\Delta M_{T_2,calc}(\%)$	ΔM_{T_2} (%)
0.0998	0.076	−34.22	-34.19 ± 0.13
0.1502	0.1249	−33.95	-34.01 ± 0.23
0.2018	0.1581	−33.91	-33.94 ± 0.17
0.2507	0.1985	−33.72	-33.74 ± 0.21
0.2997	0.2249	−33.75	-33.86 ± 0.18
0.3338	0.2309	−33.99	-34.05 ± 0.02

[a] $\Delta M_{T_2,calc}$ is the mass loss value calculated for the formation of n moles of $LiMn_2O_4$ and for the decomposition of the excess carbonates.The calculated values have to be compared with the experimental ones (ΔM_{T_2}).

$$LiMn_2O_4 \rightarrow LiMnO_2 + \left(\frac{1}{3}\right)Mn_3O_4 + \left(\frac{1}{3}\right)O_2(g) \qquad \text{(scheme C)}$$

An hypothesis on what is going on can be proposed that implies the formation within T_2 of a certain amount of $LiMn_2O_4$ and Mn_3O_4 excess. At $T > T_2$ such $LiMn_2O_4$ would decompose to $LiMnO_2$.

Actually, since ΔM_{T_2} mass losses are always greater than those calculated on the basis of simple reaction model scheme A, we have to calculate such the amount of $LiMn_2O_4$ compound from the experimental mass loss taking place at $T > T_2$ (see scheme (C)). The relationship is as follows:

$$\Delta M_{HT} = -\left(\frac{n}{3}\right)\left(\frac{M_{O_2}}{M_{tot,mix}}\right) \times 100$$

where n represents the number of moles of $LiMn_2O_4$ formed up to T_2 and that decompose at higher temperatures.

Now ΔM_{T_2} values can be calculated as the sum of the following processes:

- formation of $LiMn_2O_4$

$$\left(\frac{n}{2}\right)Li_2CO_3 + (2n)MnCO_3 + \left(\frac{3n}{4}\right)O_2(g) \rightarrow n\,LiMn_2O_4 + \left(\frac{5n}{2}\right)CO_2(g)$$

- decomposition of excess Li_2CO_3

$$\left(\frac{x_{Li} - n}{2}\right)Li_2CO_3 \rightarrow \left(\frac{x_{Li} - n}{2}\right)Li_2O + \left(\frac{x_{Li} - n}{2}\right)CO_2(g)$$

- decomposition of excess $MnCO_3$ [$1 - x_{Li} - 2n$ moles to yield the mixture Mn_3O_4/MnO with $\Delta M = -34.43\%$].

Table 6 reports the n value calculated from the ΔM_{HT} data (reported in Table 5) and the calculated mass loss which results from the sum of the three mentioned processes (see $\Delta M_{T_2,calc}$). It can be seen that the calculated values are in fair

agreement with the experimental ones. Therefore, the TGA measurements performed under nitrogen atmosphere in this composition range can be interpreted on the basis of a two stage reaction model. In the first stage the $MnCO_3$ decomposition/oxidation induces the lithium carbonate decomposition that begins to take place under 600°C (i.e below its temperature of spontaneous decomposition which is about 640°C). This results in the formation of $LiMn_2O_4$ with an excess mixture of Mn_3O_4 and MnO. Within T_2 also the residual decomposition of lithium carbonate that does not form $LiMn_2O_4$ occurs. At $T > T_2$ $LiMn_2O_4$ decomposes, with oxygen loss, yielding Mn_3O_4 and $LiMnO_2$.The model implies that, besides excess Mn_3O_4, also some free Li_2O is present. It could be surprising that no reaction takes place at temperatures in excess of 700°C between Li_2O and Mn_3O_4 or $LiMn_2O_4$. Therefore, the reaction model described so far can be refined by considering that the high temperature part of the process is actually constituted by two competing reactions:

1.

$$n_{Li_2O}Li_2O + 2n_{Li_2O}LiMn_2O_4 \rightarrow 2n_{Li_2O}Li_2Mn_2O_4 + \left(\frac{n_{Li_2O}}{2}\right)O_2(g)$$

2.

$$(n - 2n_{Li_2O})LiMn_2O_4 \rightarrow (n - 2n_{Li_2O})LiMnO_2 + \left(\frac{n - 2n_{Li_2O}}{3}\right)Mn_3O_4 + \left(\frac{n - 2n_{Li_2O}}{3}\right)O_2(g)$$

Reaction (I) is a solid state 'lithiation' of part of $LiMn_2O_4$ formed up to T_2 while reaction (II) is the mentioned $LiMn_2O_4$ thermal decomposition to $LiMnO_2$.

Table 7 reports the n_{Li_2O} $[= (x_{Li} - n)/2]$ values along with those of ΔM_I and ΔM_{II} calculated on the basis of reaction schemes (I) and (II).

It can be seen from the last column of Table 7 that the high temperature (i.e. at $T > T_2$) mass loss values calculated according to such a mixed reaction model (solid

Table 7
n_{Li_2O} is the number of free lithium oxide moles at T_2[a]

x_{Li}	n_{Li_2O}	ΔM_I	$n - 2n_{Li_2O}$	ΔM_{II}	ΔM_{I+II}	ΔH_{HT}
0.0998	0.0117	−0.18	0.0530	−0.53	−0.70	-0.76 ± 0.01
0.1502	0.0127	−0.20	0.0995	−1.03	−1.23	-1.29 ± 0.21
0.2018	0.0219	−0.35	0.1143	−1.23	−1.58	-1.70 ± 0.23
0.2507	0.0261	−0.44	0.1463	−1.64	−2.08	-2.22 ± 0.17
0.2997	0.0374	−0.65	0.1501	−1.75	−2.40	-2.62 ± 0.13
0.3338	0.0515	−0.93	0.1279	−1.53	−2.46	-2.77 ± 0.12

[a] n has the same meaning as in Table 6 ΔM_I and ΔM_{II} are the mass loss values calculated under the reaction schemes (I) and (II). Their sum is $\Delta M_{I+II}$to be compared with the experimental ones (ΔM_{HT}).

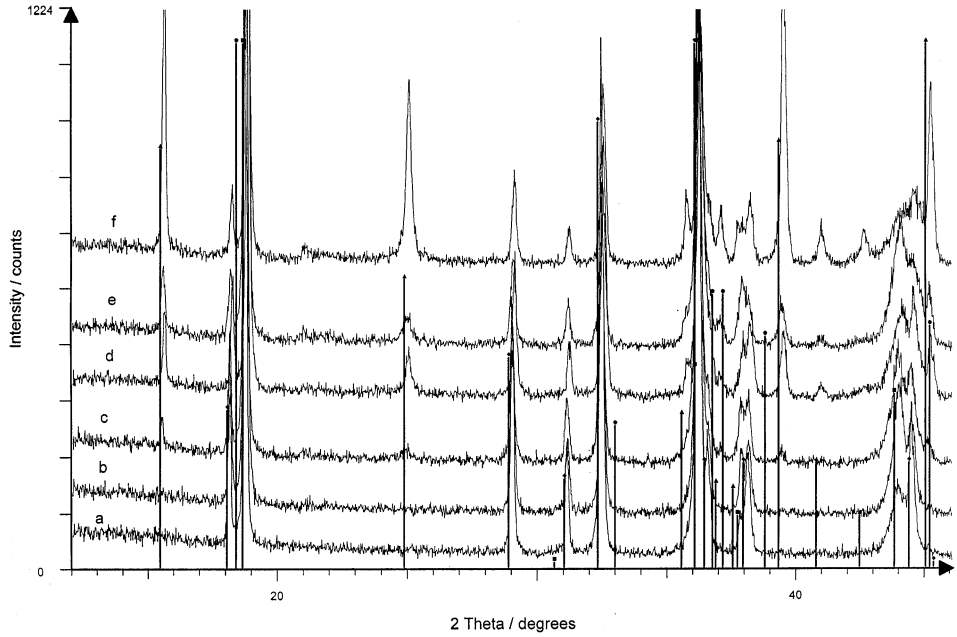

Fig. 7. XRD powder patterns of the mixtures with x_{Li} up to 0.33 and heated in flowing nitrogen to 850°C with an isothermal stage of 16 h at this temperature. (a) $x_{Li} = 0.1028$; (b) $x_{Li} = 0.1598$; (c) $x_{Li} = 0.1998$; (d) $x_{Li} = 0.2501$; (e) $x_{Li} = 0.2897$; (f) $x_{Li} = 0.3357$. Squares represent $LiMn_2O_4$ patterns (JCPDS card n. 35-0782); Circles represent $Li_2Mn_2O_4$ patterns (JCPDS card n. 38-0299); Lozenges represent Mn_3O_4 patterns (JCPDS card n. 24-0734); Triangles represent $LiMnO_2$ patterns (JCPDS card n. 35-0749).

state reaction + thermal decomposition) are in fair agreement with the correspondent experimental data (see ΔM_{HT} in Table 7).

XRD measurements have been performed on sample mixtures treated in furnace under nitrogen at 2°C min^{-1} up to 850°C + 16 h isothermal stage. The results are reported in Fig. 7. The following remarks can be made:

1. Mn_3O_4 is present in all mixtures. The intensity of the relevant peaks (marked by lozenges) show a decreasing trend with increasing x_{Li}.
2. The peaks of $LiMnO_2$ (marked by triangles) begin to be visible in the $x_{Li} = 0.20$ mixture and show an intensity which increases with x_{Li}.
3. The peak at $2\vartheta = 18.7°$ is present in the entire composition range. Such a peak cannot be univocally assigned since the most intense reflection of either $LiMn_2O_4$ (squares) and $Li_2Mn_2O_4$ (circles) falls next to this angular position.
4. A broad peak is located between about $2\theta = 35.5$ and 37.2°. In this angular range, besides the 100% Mn_3O_4 reflection and the second most intense reflection of $LiMn_2O_4$, the second most intense reflection of $Li_2Mn_2O_4$ is also located. Indeed a peak begins to appear ($2\theta \approx 37°$) in the $x_{Li} = 0.2010$ mixture which increases in the richer lithium mixtures and which can be assigned to $Li_2Mn_2O_4$. At the same composition a peak at $2\theta = 35.5°$ appears whose intensity also increases with x_{Li} and which is characteristic of $LiMnO_2$.

5. A rather wide hump is showing between $2\vartheta = 43.5$ and 45.5°. It has to be noted that in this angular range the third most intense reflection of both $Li_2Mn_2O_4$ ($2\vartheta = 45.300°$) and the 100% reflection of $LiMnO_2$ ($2\vartheta = 45.101°$) are located. Also the third most intense reflection of $LiMn_2O_4$ ($2\theta = 43.869°$) falls in this angular range. It can be seen that, starting from the $x_{Li} = 0.2010$ mixture, the peaks of $LiMn_2O_4$ are vanishing while those of $LiMnO_2$ and of $Li_2Mn_2O_4$ progressively increase.
6. Again a hump between $2\vartheta \approx 37.5$ and 39.0° is present. In this angular range, besides the fourth most intense $LiMn_2O_4$ reflection ($2\theta = 37.747°$), the fourth most intense reflection of $Li_2Mn_2O_4$ ($2\vartheta = 38.841°$) and a reflection of $LiMnO_2$ (15% relative intensity at $2\vartheta = 37.565°$) and of Mn_3O_4 (20% relative intensity at $2\vartheta = 37.983°$) are present. It seems that under this hump $LiMnO_2$ and Mn_3O_4 are the compounds which appear to have been formed.

Therefore, the XRD diffraction patterns of samples ($x_{Li} = 0.10$–0.33) treated at 850°C under nitrogen for 16 h reveal a situation where:

- Mn_3O_4 is present over all the composition range.
- $Li_2Mn_2O_4$ and $LiMnO_2$ are evident only starting from the $x_{Li} = 0.2018$ mixture and their evidence increases with x_{Li}. In the meantime the evidence of the spinel phase ($LiMn_2O_4$) disappears.
- As concerns $LiMn_2O_4$, its presence in the $x_{Li} = 0.10$ and 0.15 mixtures heated in the furnace can only be due to an higher oxygen activity with respect to that prevailing in the TGA chamber.

3.2.3. Li_2CO_3–$MnCO_3$ mixtures ($x_{Li} = 0.35$–0.50)

Table 8 reports the results of the TGA measurements performed in this composition range. The experimental data are the mean of four independent runs performed on each sample composition.

Fig. 8 reports the XRD powder patterns of the sample mixtures heated in the furnace (under nitrogen flow at 2°C min^{-1}) up to 850°C + 16 h isothermal annealing. It can be seen that Mn_3O_4 (lozenges) and $LiMnO_2$ (triangles) are the main compounds which are present. However, it has also to be noted that some other reflections are present. In particular, besides the peak at $2\theta \approx 18.5°$ (possible attribution: $LiMn_2O_4$ and Li_2MnO_3), there are diffraction effects between 20 and 22° which can only be attributed to the presence of Li_2MnO_3.

Table 8
TGA results (nitrogen flow) on the mixtures in the composition range $x_{Li} = 0.35$–0.50[a]

x_{Li}	ΔM_{T_2} (%)	T_2 (°C)	ΔM_{850} (%)
0.3501	-34.36 ± 0.25	710	-36.97 ± 0.34
0.4001	-34.64 ± 0.17	715	-37.31 ± 0.16
0.4503	-35.37 ± 0.29	716	-37.53 ± 0.40
0.5008	-35.88 ± 0.34	720	-37.88 ± 0.41

[a] The experimental mass losses at T_2 (ΔM_{T_2}) and at 850°C (ΔM_{850}) are the mean of four independent runs. T_2 is expressed in °C.

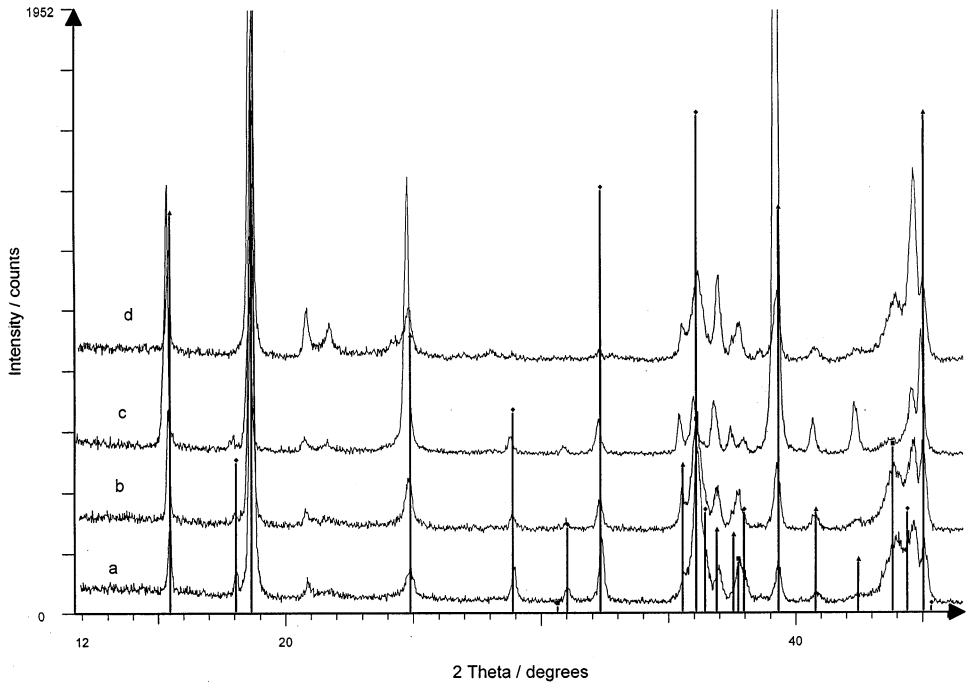

Fig. 8. XRD powder patterns of the mixtures with $x_{Li} > 0.33$ and heated in flowing nitrogen to 850°C with an isothermal stage of 16 h at this temperature. (a) $x_{Li} = 0.3520$; (b) $x_{Li} = 0.4036$; (c) $x_{Li} = 0.4607$; (d) $x_{Li} = 0.5013$. Squares represent $LiMn_2O_4$ patterns (JCPDS card n. 35-0782); Lozenges represent Mn_3O_4 patterns (JCPDS card n. 24-0734); Triangles represent $LiMnO_2$ patterns (JCPDS card n. 35-0749).

From the XRD evidence, a reaction model can be proposed according to which, up to T_2, a mixture of $LiMn_2O_4$, Li_2MnO_3 and Mn_3O_4 forms.

The reaction scheme is as follows:

$$\left(\frac{x_{Li}}{2}\right)Li_2CO_3 + (1 - x_{Li})MnCO_3 + wO_{2\,(g)} \rightarrow \left(\frac{12w - 2}{3}\right)LiMn_2O_4 + \left(\frac{2 + 3x_{Li} - 12w}{6}\right)Li_2MnO_3 + \left(\frac{4 - 3x_{Li} - 12w}{6}\right)Mn_3O_4 + \left(\frac{2 - x_{Li}}{2}\right)CO_{2\,(g)}$$

where w can be calculated from the difference between ΔM_{T_2} and the mass variation expected on the basis of carbonates decomposition. Table 9 reports the number of moles of the three compounds that should have been formed within T_2. At $T > T_2$ the following processes can take place:

$$Li_2MnO_3 + LiMn_2O_4 \rightarrow 3LiMnO_2 + (1/2)O_{2(g)} \quad (1)$$

Table 9
TGA results (nitrogen flow) on the mixtures in the composition range $x_{Li} = 0.35$–0.50[a]

x_{Li}	$LiMn_2O_4$	Li_2MnO_3	Mn_3O_4	$\Delta M_{HT,1}$	$\Delta M_{HT,2}$	$\Delta M_{HT,1} + \Delta M_{HT,2}$	ΔM_{HT}
0.3501	0.1075	0.1213	0.1045	−1.96	−0.08	−2.04	-2.61 ± 0.10
0.4001	0.1081	0.1460	0.1081	−2.07	−0.24	−2.31	-2.69 ± 0.18
0.4503	0.0748	0.1918	0.0668	−1.50	−0.78	−2.28	-2.16 ± 0.13
0.5008	0.0537	0.2235	0.0561	−1.13	−1.19	−2.32	-2.05 ± 0.30

[a] The experimental mass losses at $T > T_2$ (ΔM_{HT}, %) represent the mean of four independent runs. The number under the headings of the three compounds represent the respective moles formed up to T_2. $\Delta M_{HT,1}$ and $\Delta M_{HT,2}$ are the mass losses calculated under reactions Eq. (1) and Eq. (2) (in %).

By considering (see Table 9) that Li_2MnO_3 is always in excess, the mass loss associated to the reaction can be calculated. The $\Delta M_{HT,1}$ values are reported in the same table.

Furthermore the excess Li_2MnO_3 can react with Mn_3O_4 according to the reaction:

$$Li_2MnO_3 + (1/3)Mn_3O_4 \rightarrow 2LiMnO_2 + (1/6)O_{2(g)} \quad (2)$$

whose associated mass loss ($\Delta M_{HT,2}$) is also reported in Table 9.

The reliability of the hypothesis is indirectly confirmed by the good agreement between the experimental values ΔM_{HT} and the sum $\Delta M_{HT,1} + \Delta M_{HT,2}$. Furthermore from the calculations on the TG data, it can be easily verified that, in the case of $x_{Li} = 0.5008$ mixture, no Mn_3O_4 excess will remain at 850°C (i.e. after reactions Eqs. (1) and (2)). The XRD results (see Fig. 8d) confirm this point.

References

[1] M. Shen, A. Clearfield, J. Solid State Chem. 64 (1986) 270.
[2] M. Thackery, W.I.F. David, P.G. Bruce, J.B. Goodenough, Mater. Res. Bull. 18 (1983) 461.
[3] M. Thackery, P.J. Johnson, L.A. De Picciotto, W.I.F. David, J.B. Goodenough, Mater. Res. Bull. 19 (1984) 179.
[4] T. Ohzuku, J. Kato, K. Swai, T. Hirai, J. Electrochem. Soc. 138 (1991) 2556.
[5] M.H. Rossouw, D.C. Liles, M.M. Thackery, Mater. Res. Bull. 27 (1992) 221.
[6] J.M. Tarascon, E. Wang, F.K. Shokoshi, J. Electrochem. Soc. 138 (1991) 2859.
[7] M.N. Richard, E.W. Fuller, J.R. Dahn, Solid State Ionics 73 (1994) 81.
[8] M.F. Ryan, A. Fiedler, D. Schroder, H. Schwarz, J. Am. Chem. Soc. 117 (1995) 2033.
[9] R.J. Gummow, A. De Kock, M.M. Thackeray, Solid State Ionics 69 (1994) 59.
[10] Natl. Bur. Stand. (US) Monogr. 25, 21, 77 (1984) JCPDS 1997 card n. 35-0749.
[11] Natl. Bur. Stand. (US) Monogr. 25, 21, 78 (1984) JCPDS 1997 card n. 35-0782.
[12] J.M. Tarascon, F. Coowar, G. Amatucci, F. Shokoshi, D.G. Guyomard, J. Power Sources 54 (1995) 103.
[13] L. Crogvennec, P. Deniard, R. Brec, A. Lecerf, J. Mater. Chem. 7 (1997) 511.
[14] Zx. Shu, I.J. Davidson, R.S. McMillan, J.J. Murray, J. Power Sources 68 (1997) 618.
[15] P.G. Bruce, A.R. Armostrong, R.L. Gitzendammer, J. Mater. Chem. 9 (1999) 193.

[16] C. Masquelier, M. Tabuchi, K. Adoi, R. Kanno, Y. Kobayashi, Y. Maki, O. Nakamura, J.B. Goodenough, J. Solid State Chem. 123 (1996) 255.
[17] V. Massarotti, D. Capsoni, M. Bini, G. Chiodelli, C.B. Azzoni, M.C. Mozzati, A. Paleari, J. Solid State Chem. 131 (1997) 94.
[18] Y. Shimakawa, T. Numata, J. Tabuchi, J. Solid State Chem. 131 (1997) 138.
[19] R. Stoyanova, M. Gorova, E. Zecheva, J. Phys. Chem. Solids 61 (2000) 609.
[20] Y.J. Park, J.G. Kim, M.K. Kim, H.J. Chung, W.S. Um, M.H. Kim, H.G. Kim, J. Power Sources 76 (1998) 41.
[21] Y.H. Ikuhara, Y. Iwamoto, K. Kikuta, S. Hirano, Ceramic Trans. 83 (1998) 53.
[22] Y.H. Ikuhara, Y. Iwamoto, K. Kikuta, S. Hirano, J. Mater. Res. 14 (1999) 3102.
[23] T. Takada, H. Hayakawa, E. Akiba, J. Solid State Chem. 115 (1995) 420.
[24] T. Takada, H. Hayakawa, T. Kumagai, E. Akiba, J. Solid State Chem. 121 (1996) 79.
[25] M.M. Thackeray, M.F. Mansuetto, C.S. Johnson, J. Solid State Chem. 125 (1996) 274.